RSC Advances

ROYAL SOCIETY OF CHEMISTRY

www.rsc.org/advances

Excellent Hydrogen Evolution by a Multi Approach via Structure - Property Tailoring of Titania

Shwetharani R[a], CAN Fernando[b] and Geetha R Balakrishna[a]*

[a]Centre for Nano and Material Sciences, Jain University, Jain Global Campus, Bangalore -562112, India

[b]Nano-Technology Research Lab, Department of Electronics, Wayamba University of Sri Lanka, Kuliyapitiya, Sri Lanka

Corresponding author's full mailing address:

Dr. R. Geetha Balakrishna,

Director & Professor,

Centre for Nano and Material Sciences,

Jain University,

Jakkasandra post, Kanakapura Taluk,

Bangalore Rural district- 562112

Phone: + 91 8027577212

Fax: + 91 8027577211

cnms.jainuniversity.ac.in

*e-mail: br.geetha@jainuniversity.ac.in

Abstract:

Photocatalytic water splitting by solar energy is an ideal economic method for hydrogen generation. An attempt has been made to overcome the main barriers of photocatalytic hydrogen evolution (being rapid recombination of electron-hole pairs, the process of back reaction and poor activation of titania by visible light) by the usage of Fe induced titania. The method facilitates a cage like mesoporous structure and an effective surface level doping. The induction of dopants and formation of coupled semiconductor oxides of well matched band energy favorably contribute to the arise of mid bands and the perfect alignment of their energy levels, leading to a shallow trapping and detrapping of electrons, necessary for efficient charge separation and transfer. Decrease in band gap energy to ~ 2.0 eV and hence the extended light absorption in modified titania, together with a shift in band edge potentials (caused by pH variation), results in an activated titania, desired for enhanced visible light hydrogen evolution. The modified nanostructure shows an excellent hydrogen evolution of 255 mmol/g/h, one of the highest reported so far. Sodium acetate acts as a good sacrificial agent in preventing the back reaction. Characterization techniques like spectroscopy (XRD, UV, reflectance, EDX, XPS and PL) and microscopy (FESEM and HRTEM) have been used to evidence the presence of Fe as dopant/ as oxide and to study the structure property tailoring that occurs in the chemical modification.

Keywords: Photocatalyst, Fe-TiO_2, Hydrogen generation, water reduction, visible light, Renewable energy.

1. Introduction:

Hydrogen is no doubt an ideal and renewable energy source in future because of its clean nature and being energy efficient. Nature relies on photocatalysis to store energy and we can follow its example to produce hydrogen from water. Photocatalysis is known to be the most economic route to evolve hydrogen [1]. Several photocatalysts have been shown to split water into hydrogen and oxygen using light. The three requirements for the photocatalytic hydrogen production are, a) the photocatalyst must have a band gap of at least ≈1.23 eV (the necessary thermodynamic potential for water splitting) although the over potential due to slow reactions and resistance in the system make the required band gap closer to 1.7-1.8 eV b) the conduction band of photocatalyst must be more negative than the redox potential of H^+/H_2O (0 V Vs NHE) and valence band edge should be more positive than the redox potential of O_2/H_2O (1.23 eV) for an efficient H_2 and O_2 evolution c) stability of the photocatalyst must be sufficiently good in aqueous conditions without any deactivation. TiO_2 is the most common photocatalyst which satisfies the above requirements and hence is envisaged to be the best agent for hydrogen generation. It has high resistance to corrosion and is cheap, easily available and environmental friendly. Fujishima and Honda have demonstrated the photoinduced decomposition of water on TiO_2 electrode [2] for the first time in 1972 [3] and have reported a very small amount of hydrogen release (4-5 μmol/g/h). It is only in 2009 and onwards that such studies have been concentrated to explore the potency of hydrogen being generated as an alternative source of energy to support the depleting energy source. Titanium dioxide when irradiated with photons of wavelength ≤ 400 nm generates electron-hole pairs in the conduction and valence band respectively. The band edge potentials and the band energy are sufficient enough to overcome

the endothermic character of the water splitting reaction. The activated electron in the conduction band reduces the adsorbed H^+ and oxygen to produce H_2 or $OH^{\bullet -}$ and $OH^{\bullet}$ respectively, and when OH species/radicals are scavenged by appropriate reducing species, it facilitates the overall hydrogen evolution. TiO_2 typically absorbs ultraviolet light, to conquer its wide band gap energy (~ 3.2 eV for anatase phase) for photocatalytic hydrogen generation [4]. Since the total solar spectrum encompasses only ~ 5-10 % of the UV radiation [5-6], it is still challenging to apply TiO_2 for large scale production. Also the limitation of highly probable recombinations occurring in the above photocatalyst and ultra fast hole transfer processes that can cause back reaction of H_2 and O_2 to water, add to the above challenges. Several modifications were designed to obtain an apt product/ process to overcome the above challenges such as doping of transition metal ions, non metal elemental doping, addition of sacrificial agent (SA), photosensitizers, coupling with other semiconductor oxides and ion implantation (expensive and possible only in the high crystalline TiO_2) [7-10]. Formation of doped and composites of TiO_2 have observed to be one of the promising strategy to sensitize TiO_2 to visible light. Among various dopants, Fe is considered to be an attractive candidate to enhance the water splitting photocatalytic reaction. Also Fe^{3+} ion has an ionic radius (0.645 Å) comparable to that of Ti^{4+} (0.68 Å) and it is energetically favorable for Fe^{3+} ion to occupy Ti^{4+} sites substitutionally. The created energy levels of dopants lie closer to conduction and the valence band edge of TiO_2. In the composite of TiO_2 and Fe_2O_3, the valence band of Fe in Fe_2O_3 is less positive than the valence band edge of TiO_2 and can easily act as an electron acceptor placing itself at a potential of 2.4 eV, with respect to NHE [11-13]. Absorption of visible light equivalent to 2.6 eV allows electron excitation from O 2p of Fe_2O_3 to 3d of Ti. Fe t_{2g} level is located at 0.2 eV above the valence band and Fe eg level is split into d_z^2 and $d_{x^2-y^2}$ orbital's which extend the conduction band to some degree. Fe^{3+} ions act as shallow

traps in the TiO_2 lattice, to decrease the recombination of electrons and holes and hence to enhance the photocatalytic efficiency. Fe ions can hence not only trap electrons but also holes. It is both an electron/ hole recombination inhibitor and an efficient electron transfer agent [14-15]. However the regenerative behavior of Fe^{3+}/Fe^{2+} couple is undesirable and can deplete H^+ ions contributing to low yield of hydrogen. SA plays a very important role in capturing the holes (h^+), thus allowing the electron for reduction of protons to hydrogen and cause hydrogen evolution. The polarity, oxidation potential and adsorption ability of SA need to be evaluated before their selection for the process.

Although Fe doped titania is synthesized by impregnation method for hydrogen evolution by various groups, the amount of hydrogen evolved remains at micro level, the present paper reports the use of new precursors with an efficient SA to evolve a high concentration of hydrogen (milli mole). It has been reported that $FeTiO_2$ synthesized by impregnation method (band edge at 366 nm) shows 4-5 μmoles/g/h of hydrogen release from water containing EDTA solution [4] and further 270 μmoles/g/h by a modified wet impregnation method (band edge at 575 nm) [16]. Similarly the same photocatalyst when prepared by hydrothermal method by Alam khan et al. [17] has been observed to release 125 μmoles/g/h of hydrogen. The literature reports higher activity with 0.2 – 1 % of iron content as dopant and when the iron exceeds 2 %, it results in a net decrease in activity. Another important parameter like calcination observes to play a prominent role in hydrogen evolution [18-19]. Higher calcination temperatures have been reported to increase crystallinity leading to lesser defects. Excess defects tend to act as recombination centers [20]. The present article demonstrates the synthesis of $FeTiO_2$ nanostructure using wet impregnation method at high calcination temperature for a significant and improved production of hydrogen. The technique involves spinning of the dopant precursor

with TiO_2 at a high speed in aqueous condition so that the kinetic energy involved is high enough to induce lattice atomic relocation mostly on the surface of TiO_2 atoms. Excess precursor results in aggregate oxides which tend to deposit on surface as oxides when calcined. A feasible precursor which could positively result in Fe_2O_3, which further diffuses/adsorbs on TiO_2 to form a desirable structure of $FeTiO_2$ and its iron oxide composite (with enhanced properties) respectively, was carefully selected. Different dopant concentrations and pH conditions were experimented for optimized formulation and process. The pH of the solution greatly influences the surface charge and band edge positions of the semiconductor particles and, studies at different pH conditions give a deep insight of the events occurring on the surface of the reaction. Hence a sustainable, high hydrogen production is aimed by a multi approach via photocatalytic water reduction, solving energy and environment issues.

2. Experimental:

2.1 Photocatalyst preparation:

Commercially available (CM) Sd fine TiO_2 was directly used as TiO_2 source and Fe $(NO_3)_3$ $6H_2O$ (98 % Merck) as Fe source for the preparation of $FeTiO_2$. To obtain 0.15 % $FeTiO_2$, the aqueous mixture of TiO_2 and Fe $(NO_3)_3$ were stirred at 60° C for 24 h to form the corresponding doped sample of composition $Ti_{0.85}\,Fe_{0.15}\,O_{2.0}$. The obtained sample was dried at 100° C and then calcined at 600° C for 5 h to obtain an anatase phase of the nanoparticles. The powders (doped and undoped) were then pulverized using a Spex mixer mill with an agate vial for an hour and used for the photocatalytic reactions. Different precursor concentration resulted in proportionate dopant concentration in titania. Concentrations ranging from 0.05, 0.1, 0.15, 0.2 and 0.25 % were experimented and photocatalytically evaluated. 0.15 % of Fe doping was observed to be

optimum. Increase of dopant concentration beyond a proportion limit caused an adverse effect as shown in Figure 1 of supporting information (SI). When Fe^{3+} ion concentration exceeds the optimum level, there appears to be a tendency of disturbance in the titania framework leading to adverse photocatalysis [21]. The present work focuses on complete characterization of an optimally (0.15 %) doped titania and evaluation of its photocatalytic efficiency as a water reduction agent.

2.2 Photocatalyst Characterization:

Powder X-ray diffraction pattern was recorded for phase identification from a P analytical X'pert pro diffractometer with Cu Kα radiation (secondary graphite monochromator) at a scan rate of 1°/min. The crystallite size and the lattice parameters were calculated using Debye-Scherrer equation [22] and $1/d^2 = h^2/a^2 + k^2/b^2 + l^2/c^2$ where d is the distance between the crystal planes of hkl indices and a, b, c are the lattice parameters. Field emission scanning electron microscopy (FE-SEM) images were obtained by Carl zeiss supra-55 field emission microscope using an acceleration voltage of 20 kV. Energy-dispersive X-ray analysis (EDX) was used in conjunction with scanning electron microscopy to study the surface morphology and to detect the elements in the prepared samples. The absorption spectrum was recorded for nanomolar suspensions of the photocatalyst prepared by milling to avoid the reflection of light to a maximum extent, using a Shimadzu 1700 PC UV-visible spectrophotometer. The surface area of the catalyst was determined by a Smart Sorb 93 Brunauer – Emmett – Teller (BET) surface analyzer with sorb 93 reduction software. The high resolution transmission electron microscopy (HRTEM) images were obtained from JEM-2010 electron microscope (JEOL, Tokyo, Japan) at an accelerating voltage of 200 kV. TGA-DTA analysis was performed (TGA Q50 V20.13 Build 39) in a

temperature range of 35-700°C. Photoluminescence (PL) experiments were performed on a Shimadzu RF 5301 PC spectrofluorometer.

2.3 Photocatalytic hydrogen production:

At first 5 mg of $FeTiO_2$ semiconductor particulate system was dispersed in 250 ml of water with 0.5 M concentration of sodium acetate as sacrificial agent solution in a reactor set up as shown in Fig 1. Before irradiation Ar was flushed opening the inlet valves-7 and 11 to remove dissolved H_2 up to almost zero ppm level in the fully covered reactor cell as shown in Fig.1. During the illumination valves-7 and 11 were closed properly preventing the dissolution of H_2 into the environment. 100 W tungsten lamp (Phillips) with a photon flux of 10mW cm^{-2} which peaks around 800 - 850 nm was used with a cutoff filter to remove any thermal radiation and to ensure illumination by visible light over an exposure area of 30 cm^2. Ar was flushed continuously at a very slow rate collecting the produced H_2 in the upper circulating loop, having the circulation pump to send the H_2/Ar mixture into the GC from the outlet valve-6, each time in a 4 min cycle. Sodium hydroxide is used to cause the necessary increase in pH values.

3. Results and Discussion:

3.1 Structural and Morphological analysis:

Figure 2 shows the XRD pattern of the $FeTiO_2$ sample calcined at 600° C. The diffraction pattern exhibits characteristic reflections for tetragonal anatase phase of titania, with intense peaks at 2θ corresponding to 25.3°; 37.8°; 48.0°; 53.9°; 55.0° and 62.7° for the (1 0 1); (0 0 4); (2 0 0); (1 0 5); (2 1 1) and (2 0 4) reflections respectively, in agreement with JCPDS no. 21-1272. The appearance of peaks at 33.15° (104) and 35.65° (110) indicates a new phase of iron oxide and this suggests the chance of iron oxide (Figure 2 of SI) being dispersed on the surface of TiO_2

grains or in between the interfaces of TiO_2 agglomerates, in addition to lattice substitution of Fe in TiO_2 [23-24]. The pre adsorbed Fe precursor is decomposed during calcination and the same present on the surface, allows easy diffusion and adsorption of Fe and iron oxide respectively onto the TiO_2, producing a mixture of $FeTiO_2$ and iron oxide /TiO_2 solid solution. Surface doping and surface adsorption facilitates easy electron transfer to active sites for H^+ reduction. Table 1 gives the cell volume, surface area and the average crystallite sizes, calculated by Scherrer equation for the most intense diffraction peak at $2\theta=25.33°$. Cell volume increases on doping, indicating the presence of defects/ oxygen vacancies (Vo) present in the doped sample. Crystallite size and surface area is observed to be contrary and doubled on doping, indicating better interaction of water molecules with the photocatalyst more so in the visible light. Anatase phase was prominently observed without rutile or brookite phase. Several studies on Fe doped TiO_2 photocatalyst systems have revealed that Fe^{3+} enters the TiO_2 lattice substitutionally due to similar ionic radius with more solubility in anatase phase compared to the rutile phase [25]. FESEM images in Fig 3 depict the morphology of the synthesized nanostructures. The particles appear to be smooth and uniformly distributed throughout, with a porous network of nano-spheroids, facilitating better water adsorption, penetration and photoreaction as compared to bare titania (Fig 3a of SI). Morphology of cage like structure with high surface area (marked in circles in Fig 3) provides easy access of more water molecules to the photocatalyst, enhancing hydrogen production. The high resolution TEM images gives well resolved lattice planes of $FeTiO_2$ nanostructure as shown in Fig 4, in which the facet distances of 0.37 nm and 0.25 nm correspond to (101) plane of anatase TiO_2 and (110) plane of Fe nanoparticles respectively (Fig 4a and 4b) [26]. The corresponding SAED (selective area electron diffraction) pattern (Inset in Fig 4b) of discrete nanoparticles indicate more intense spots and speckled pattern due to the large grain size

(obtained at higher calcination temperature) and polycrystalline anatase structure. Figure 4c shows the dislocation fringe spacing (showed in arrows) due to addition of the dopant element Fe. Dopant increases lattice strain, which will anchor dislocation (crystallographic defect) in lattice fringes confirming the effect of modification in titanium dioxide nanoparticle [27]. The particle size averages in the range of 60-70 nm (inset in Fig 4d). The morphology clearly indicates some irregular shaped particles, attributed to substitution (Fig 4d)/ adsorption (Fig 4e and indicated in colored arrows) of Fe/ iron oxide respectively on titania unlike the bare titania (Fig 3b of SI). The dark regions indicate the overlie of particles one above the other (Fig 4f).

3.2 Elemental analysis:

Figure 5 shows the elemental composition of the doped sample analyzed by EDX. It shows peaks for Ti, O and Fe elements and indicates the absence of other impurity. Inset shows the atomic and elemental percentage of the dopant in titanium dioxide. The obtained composition $Ti_{0.81}$ $Fe_{0.12}$ $O_{2.07}$ is in agreement with the proposed percent (0.15 %) of dopant concentration. Figure 6 depicts the high resolution XPS spectra of $FeTiO_2$ photocatalyst. Wide XPS spectrum of Fe-TiO_2 photocatalyst, which indicates the presence of Ti, O and Fe at various binding energy levels are indicated in Fig 6a. The binding energies 459.5 eV and 465.3 eV in Fig 6b corresponds to Ti 2p core level spectrum and is in agreement with literature reports [28]. The slight shift of Ti $2p_{3/2}$ peak with respect to that of Ti^{4+} in pure anatase TiO_2, i.e. from 458.5 to 459.7 eV indicates the presence of Ti^{3+}. The main peak for O 1S at about 530.7 eV is as shown in Fig 6c and is attributed to the lattice oxygen in the metal oxide (Ti-O, Fe-O) [29-30]. Figure 6d shows the Fe 2p core level spectrum. The peaks of Fe are very weak due to the low dopant concentration. The binding energies located at around 712 eV and 724 eV could be assigned to the trivalent oxidation state of Fe^{3+} $2p_{3/2}$ and Fe^{3+} $2p_{1/2}$ respectively and Fe 2p doublet implied the presence of

Fe-O bonds [31]. Thus the XPS analysis substantiates the presence of Ti^{3+} defect, Ti-O and Fe-O bonds in the Fe induced titania sample.

3.3 Optical and Spectral analysis:

Figure 7 depicts the UV-visible absorption spectra of the catalysts. The slightly red colored $FeTiO_2$ shows an extended red shift and an increased visible light absorption in contrast to commercially available TiO_2, which shows an absorption threshold at ~ 400 nm. Increase in dopant concentration up to 0.15 % extends the absorption threshold to 600 nm, beyond which a decrease is observed. The surface barrier and space charge region should be synergistic for efficient trapping and transfer of electrons, and beyond the optimum concentration the possibility of trapped charge carrier recombination through quantum tunneling would be more with the lack of driving force to separate them. For higher dopant concentration space charge region becomes very narrow and the penetration depth of light into TiO_2 greatly exceeds the thikness of space charge layer, enhancing the rate of recombination of electrons and holes. Concentration of induced ion become optimum when the thickness of the space charge layer equals the depth of light penetration. The red shift from 400 nm to 600 nm may be attributed to the mid band created by Fe^{3+} which shifts the optical absorption edge of crystal to higher wavelength (visible region) in the doped sample. The electronic transitions from the valence band to the dopant level or from the dopant level to the conduction band can efficiently red shift the band gap energy absorption threshold [32] to obtain a band gap of ~ 2 eV. The mid bands could also be due to the distortions related to defect centers caused in the process of doping. Coupled semiconductors of well matched band energies as in the case with TiO_2 and iron oxide are favorable to improve charge separation and transfer [33]. A better charge separation in the coupled system is the result of fast electron transfer process between the two semiconductors. The vectorial nature of electron gives

cascading of electron from TiO_2 to Fe_2O_3 leading to a better process of charge separation [34]. Figure 8 depicts the reflectance spectra of $FeTiO_2$, with a broad absorption ranging from 415 nm to 570 nm indicating d–d transitions of either transition metal impurity or a chromophoric group (due to one of the native defects) or both [35]. Fe^{3+} ions are substitutionally located in Ti^{4+} lattice site with and without charge compensation by oxygen vacancy at a nearest neighbor site of 0.08 eV below the energy level of conduction band [36]. Theoretical calculations show that a high vacancy could induce a vacancy band of electronic states just below the conduction band.

Formation of doped titania/ composite oxides led to changes in charge carrier trapping, immigration and transfer and is substantiated by photoluminescence (PL) studies. The PL emission observed in any semiconductor originates mostly from radiative recombinations that occur between the photo-generated electrons and holes. When the semiconductor is excited by light equivalent to its band gap energy, the photo-generated electrons on reaching the conduction band return back to the valence band, with a discharge of energy as photoluminescence radiation. This process is recognized as direct band–band transition photoluminescence. In the other photoluminescence process, the excited electrons firstly transfer from the conduction band to different sub-bands, e.g. surface oxygen vacancies or defects, via non-radiative transition, and subsequently transfer from the sub-bands to the valence band via radiative transition with the release of photoluminescence signals [37]. Figure 9 shows the PL spectra of the TiO_2 and Fe-TiO_2 nanostructures. TiO_2 nanoparticles show the emission peak at 450 nm. This characteristic broad band of anatase crystals is due to the radiative recombination of self trapped excitons [38]. On doping, the PL emission is extremely decreased and indicates a delay in recombination rate suggesting the increased availability of electrons for good hydrogen production [39]. The small emissions at 390, 413 and 434 nm are attributed to the recombination of trapped electrons/ holes

in surface defects. The emission peak at around 462 nm (indicated by arrows) corresponds to mid band or deep level traps caused by Fe incorporation into TiO_2, which can in turn cause delayed recombination. The induction of trivalent ion (Fe^{3+}/Ti^{3+}) introduces oxygen vacancies and/or interstitial cations (Fe^{3+}, Ti^{3+}, and Ti^{4+}), to spontaneously maintain charge neutrality or equilibrium [40]. These defect states may be due to the Fe^{3+} - Vo and Ti^{3+} - Vo. The lattice defects can raise the fermi level of TiO_2, correspondingly to increase the height of the potential barriers that repel electrons to the surface, thus reducing the rate of recombination of electrons and holes [41]. If the ions have valences greater than three as Ti^{4+} in TiO_2, cation vacancies tend to form and the presence of such cation vacancies are better tolerated in an anatase structure, due to the better charge defect compensation by the neighboring Ti cations [42].

Addition of SA, sodium acetate decreases the PL emission all the more, due to further lowering of recombination. Sodium acetate being a well known SA scavenges holes, decreases recombination, thus contributing to more availability of electrons for hydrogen evolution (as shown below).

$$\mathbf{2CH_3COO^- + 2h^+ \longrightarrow C_2H_6 + CO_2}$$

Thermo gravimetric analysis (TGA) and differential thermal analysis (DTA) was carried out to substantiate the stability of the photocatalyst. Fig 4 in SI shows TGA-DTA curves for the prepared $FeTiO_2$ after being used and regenerated (annealed at 600° C) after one cycle of hydrogen evolution (40 mins). In TGA curve, a weight loss of 0.2 % was observed in the temperature range between 37 to 230° C, while the DTA curve displayed an endothermic peak centering at 42° C and is ascribed to dehydration and loss of water molecules [43]. An exothermic peak around 380-400° C indicates the crystallization temperature and phase change

of the photocatalyst to anatase phase. The large particle size lowers the crystallization temperature [44]. There is no considerable weight loss (total weight loss is about 0.2 %) with respect to temperature changes and this indicates the prepared $FeTiO_2$ to be thermally stable and reusable. Further XRD, UV and PL spectra of the doped sample as depicted in Fig 5 of SI, before and after five cycles of hydrogen evolution, reveal similar patterns confirming the undisturbed lattice structure and stability after repeated use.

The electronic structure of the modified titania has hence been observed to be influenced by crystal structure, crystallite size (increase), surface morphology (nanocrystalline structure) and can be well correlated to its electronic and optical property, to study its enhanced photocatalytic capacity to split water and evolve hydrogen.

3.4 Photocatalytic hydrogen evolution:

The prepared nanomaterial was evaluated for its efficiency as photocatalyst to cause water reduction and hydrogen evolution under visible light irradiation (tungsten source). The efficiency of a metal ion (as in a doped sample/ composite iron oxide) to induce enhanced photoreaction depends on whether it serves as a mediator of interfacial charge transfer or as a recombination center. The efficiency of the photocatalyst then further depends on much more intricate parameters such as the dopant concentration, its electronic configuration, their energy levels and the distribution of the dopants with in the particles. As mentioned earlier 0.15 by atom percent of Fe gives the optimum evolution of hydrogen. The above formulation was observed to give a maximum extension of light absorption into the visible range (600 nm) as confirmed by UV-visible spectra (Fig 7). Doping causes mid bands which decreases the band gap energy to visible range. Figure 10 shows the H_2 evolution from visible light mediated catalytic water reduction

using $FeTiO_2$ (0.15 %, Fe) at different pH conditions. A remarkable H_2 evolution rate of 255 mmol/g/h with a quantum efficiency [45, 46] of 39.7 % was observed in the visible region from this system when compared to presently available literature. The average solar to hydrogen efficiency [47] of 6.4 % is obtained as per the equation below,

STH % = {Output energy of hydrogen evolved $_{AM\ 1:5G}$ / Energy of incident solar light} x 100

$$STH\ (\%) = \left\{ \frac{\text{mmol } H_2/\text{s X 237 (kJ/ mol)}}{P_m\ (MW/cm^2)\ X\ \text{Area } (cm^2)} \right\} X\ 100$$

The mechanism of visible light activity of Fe induced titania can be explained based on its energy band potentials. Fe doped nano-titania consists of a broad Ti 3d and a sharp Fe 3d orbitals as the conduction band and the O 2p as the valence band of TiO_2 [17]. The composite of Fe_2O_3-TiO_2 consists of an additional O 2p of Fe_2O_3 as the valence band. On the basis of the results, a band structure for synthesized sample is as shown in Scheme 1, it is suggested that electron-hole pairs are generated under visible light illumination and the electrons are transferred by three approaches, a) from valence band of $FeTiO_2$ to Fe 3d level, when the energy of photon is $\geq E_{Fe\ 3d} - E_V$, b) from the valence band of O 2p of Fe_2O_3 into Fe 3d level, when the energy of photon is $\geq E_C - E_V$, c) from the valence band of Fe_2O_3 to Ti 3d, when the energy of photon is $\geq E_{Ti\ 3d} - E_V$, d) and also excitation of electron from Fe 3d band to conduction band of Ti, when the energy of photon is $\geq E_C - E_{Fe\ 3d}$. In addition there can also be a transfer of electron from O 2p of $FeTiO_2$ to O 2p of Fe_2O_3, which acts as good acceptor (A) level placed at a potential of 2.4 eV, when photon energy is $\geq E_A - E_V$, causing holes in Ti valence band. These holes are then scavenged by a pre adsorbed SA to avoid the back reaction. The presence of mid bands/ vacancies/ defect sites (Fe^{3+} mid band, Ti^{3+} - Vo, Fe^{3+} - Vo,) adds to good electron transfer and charge separation. The

trapped electrons in the above mentioned energy states are then detrapped, transported to the reaction site at the surface, efficiently resulting in a much higher hydrogen production. The reduced recombination on doping is strongly evident by PL studies which display a decrease in PL emission [48]. Thus the efficient charge separation (reduced electron hole recombination) and visible light activity (substantiated by UV-Vis spectroscopy) due to the dopant/ composite is justified.

The decomposition of water into hydrogen and oxygen is a chemical reaction with large positive Gibbs free energy (ΔG= 237 kJ/mol) and thus the back reaction is very facile. SA favorably scavenges holes to avoid the back reaction in the above water reduction reaction. The efficacy of SA in such photocatalytic water reduction reactions depends on, a) the extent of pre adsorption of SA on to the surface of TiO_2 b) its reduction potential (the measure of thermodynamic ability to reduce the photogenerated hole in photocatalyst) and c) the kinetic barrier for electron transfer process. The optimum amount of 0.5 M sodium acetate has been used as a SA. In order to facilitate the direct electron transfer from the SA to TiO_2, attachment of SA to TiO_2 surface is one of the primary requirement. Also the two polar OH groups in sodium acetate [– (C – O)] reduces the kinetic barrier for electron transfer from sodium acetate to TiO_2 (termed as reductive quenching). It is substantiated and can be confirmed from PL studies, that least amount of charge carrier recombination occurs when SA is used with modified titania for water reduction reaction. Carbonyl species can effectively suppress the back reaction and activate the photo absorption of oxygen on TiO_2. Sodium acetate is hence a hole scavenger, through indirect reduction of h^+ to form the reducing species $CO_2^{-\bullet}$.

It is observed that increase in pH enhances H_2 evolution rate. Change in pH causes change in semiconductor flat band potential due to the change in the adsorbed charge (H+ and

OH-) on the electrode surface. Addition of negative charge (OH^- ions) shifts the band to a more negative potential, where as adsorption of a positive charge (such as H^+ ions) shifts it to the positive potential [49]. When the onset shifts towards negative potential, it supports the shift of conduction band position of TiO_2 towards more negative side so as to produce a higher driving force for electron transfer to the H^+/H_2O redox level, efficiently contributing to hydrogen evolution. The photocurrent on-set potentials obtained from $FeTiO_2$ powder pressed on to a conductive glass plate shows that the flat band potential (approximately equal to the on-set potential) becomes more negative with increase in pH and has a value sufficient for photo-reduction of water. Flat band potentials obtained for the photo-electrode were -0.15 V, -0.12 V and 0.11 V vs NHE at pH=10, 8 and 6 respectively. In all it can be stated that " a perfect alignment of the energy levels lead to a shallow trapping and detrapping of electrons, necessary for efficient charge separation and electron transfer. The decrease in band gap energy to ~ 2.0 eV and hence the extended light absorption in modified titania, together with a shift in band edge potentials (caused by pH variation), results in an activated titania, desired for enhanced visible light hydrogen evolution".

It is important to mention that the present group has earlier performed a comparative study of photocatalytic oxidative degradation with two sources of light, tungsten and sunlight. The observations indicate that the sunlight is more effective in causing photocatatytic oxidations by ≈ 4.5 times over tungsten light [50]. Hence it is reasonable to presume that if a photocatalytic reactor is aptly designed to harvest sunlight, then it can cause much more enhanced water reduction and economic hydrogen evolution. However the present investigating group is working on this and shall soon communicate it as a follow up work of this.

4. Conclusions:

The present study reports the synthesis of 0.15 % Fe induced titania nanostructure, at high calcination temperature through wet impregnation technique. The Fe induced titania posses a highly reactive tetragonal anatase phase with dispersed nanospheroid structure desired for high interaction of water molecules with the photocatalyst. It shows a remarkably high photocatalytic capacity to evolve hydrogen, to an extent of 850 μmoles/5mg within 40 mins. The Fe^{3+}/ defects/ oxygen vacancies create mid bands (0.2 eV wrt NHE)) between conduction and valence band of titanium dioxide causing a favorable alignment of band edge for an efficient electron generation, separation and transfer on absorption of visible light. The created mid bands contribute to an efficient charge trapping and reduced recombination. Applying optimum pH of 10 facilitates favorable alignment of band edges towards negative potential to enhance the redox potential necessary, for water reduction.

5. Acknowledgements:

The authors greatly acknowledge Jain University for the financial support and Wayamba University of Sri Lanka.

6. References:

[1] H. Wender, R. V. Gonçalves, C.B. Dias, M. J. M. Zapata, L. F. Zagonel, E. C. Mendonça, S. R. Teixeira and Fl´avio Garcia, *Nanoscale*., 2013, 5, 9310.

[2] A. Fujishima and K. Honda, *Nature*., 1972, 238, 37.

[3] S. T. Martin, H. Herrmannt and M. R. Hoffmann, *J. Chem. Soc. Faraday Trans*., 1994, 90(21), 3323.

[4] H. Choi, M. G. Antoniou, M. Pelaez, A. A. De la Cruz, J. A. Shoemaker and D. D. Dionysiou, *Environ. Sci. Technol*., 2007, 41, 7530.

[5] C. Belver, R. Bellod, A. Fuerte and M. Fernandez Garcia, *Appl. Catal. B Environ.,* 2006, 65, 301.

[6] J. L. Gole, J. D. Stout, C. Burda, Y. Lou and X. Chen, *J. Phys. Chem. B.,* 2004, 108 (4), 1230.

[7] M. Anpo , Y. Yamashita and Y. Ichihashi, *Optronics.,* 1997, 186, 161.

[8] M. Anpo, *Pure Appl Chem.,* 2000, 72, 1265.

[9] M. Anpo and M. Takeuchi, *Int J Photoenergy.,* 2001, 3, 89.

[10] H. Yamashita, M. Harada, J. Misaka, M. Takeuchi, Y. Ichihashi and F. Goto, *J Synchrotron Radiat.,* 2001, 8, 569.

[11] J. A. Navio, M. Macias, M. Gonzalez-Catalan and A. Justo, *J Mater Sci.,* 1992, 27, 3036.

[12] R. I. Bickley, J. S. Lees, R. J. D. Tilley, L. Palmisano and M. Schiavello, *J Chem Soc Faraday Trans.,* 1992, 88, 377.

[13] W. Choi, A. Termin and M. R. Hoffmann, *J Phys Chem.,* 1994, 98, 13669.

[14] K. Ranjit and B. Viswanathan, *J Photochem Photobiol A Chem.,* 1997, 108, 79.

[15] S. Ikeda, N. Sugiyama, S. Murakami, H. Kominami, Y. Kera and H. Noguchi, *Phys Chem Chem Phys.,* 2003, 5, 778.

[16] J. K. Reddy, K. Lalitha, P. V. L. Reddy, G. Sadanandam, M. Subrahmanyam and V. D. Kumari, *Catal Lett.,* 2014, 144, 340.

[17] M. Alam Khana, S. I. Woob and O. Yanga, *Int. J. Hydrogen Energy.,* 2008, 33, 5345.

[18] Akihiko Kudo and Yugo Miseki, *Chem. Soc. Rev.,* 2009, 38, 253.

[19] Y. Wang, H. Cheng, Y. Hao, J. Ma, W. Li and S. Cai, *J. Mater. Sci. Lett.,* 1999, 34, 3721.

[20] V. Jagadeesh Babu, S. Vempati and S. Ramakrishna, *RSC Adv.,* 2014, 4, 27979.

[21] S. Ikeda, N. Sugiyama, S. Murakami, H. Kominami, Y. Kera and H. Noguchi, *Phys Chem Chem Phys.,* 2003, 5, 778.

[22] R. Shwetharani, M. S. Jyothi, P. D. Laveena and R. Geetha Balakrishna, *Photochem. Photobiol.,* 2014, 90(5), 1099.

[23] Q. Xiang, J. Yu and M. Jaroniec, *J. Am. Chem. Soc.,* 2012, 134, 6575.

[24] S. K. Sahoo, K. Agarwal , A. K. Singh, B. G. Polke and K. C. Raha, *IJEST.,* 2010, 2(8), 118.

[25] J. Araña, O. González D´ıaz, M. Miranda Saracho, J. M. Doña Rodr´ıguez, J. A. Herrera Melián and J. Pérez Peña, *Appl. Catal. B.,* 2001, 32, 49.

[26] H. Zhu, E. Zhu, G. Ou, L. Gao and J. Chen, *Nanoscale Res Lett.,* 2010, 5, 1755.

[27] D. B. Williams and C. Barry Carter, Transmission electron microscopy Part-1 basics, second edition, Springer, New York, 2009.

[28] L. Deng, S. Wang, D. Liu, B. Zhu, W. Huang, S. Wu and S. Zhang, *Catal Lett.,* 2009, 129, 513.

[29] C. Shifu, Y. Xiaoling and L. Wei, *ECS Trans*., 2009, 21(1), 3.

[30] M. I. Litter and J. A. Navfo, *J. Photochem. Photobiol. A.,* 1996, 98, 171.

[31] N. T. K Thanh, Magnetic Nanoparticles: From Fabrication to Clinical Application, CRC press, 2012.

[32] S. George, S. Pokhrel, Z. Ji , B. L. Henderson , T. Xia, L. Li, J. I. Zink, A. E. Nel and L. Mädler, *J Am Chem Soc.,* 2011, 133(29), 11270.

[33] A. Elaziouti, N. Laouedj, A. Bekka and R. N. Vannier, *J King Saud Univ Sci.,* 2014, 10.1016/j.jksus.2014.08.002.

[34] C. Nasr, P.V. Kamat and S. Hotchandani, *J. Phys. Chem. B.,* 1998, 102, 10047.

[35] Y. Ma, X. Wang, Y. Jia, X. Chen, H. Han and C. Li, *Chem. Rev.,* 2014, 114, 9987.

[36] J. Moser and M. Gratzel, *Helv. Chim. Acta.,* 1987, 70, 1596.

[37] J. Yan, G. Wu, N. Guan, L. Li, Z. Lib and X. Caob, *Phys. Chem. Chem. Phys.,* 2013, 15, 10978.

[38] W. F. Zhang, M. S. Zhang, Z. Yin and Q. Chen, *Appl. Phys. B.,* 2000, 70, 261.

[39] Y. Wang, Q. Lai, F. Zhang, X. Shen, M. Fan, Y. Heae and S. Renf, *RSC Adv.,* 2014, 4, 44442.

[40] W. Hung, S. Fu, J. Tseng , H. Chu and T. Ko, *Chemosphere.,* 2007, 66, 2142.

[41] A. Heller, Y. Degani, D. W. Johnson and P. K. Gallogher, *J. Phys chem.,* 1987, 91, 5987.

[42] X. H. Wang, J. G. Li, H. Kamiyama, M. Katada, N. Ohashi, Y. Moriyoshi and T. Ishigaki, *J. Am. Chem. Soc.,* 2005, 127, 10982.

[43] A. Abidov, B. Allabergenov, J. Lee, H. Jeon, S. Jeong and S. Kim, *IJMMM.,* 2013, 1(3) , 294.

[44] N. Hafizah and I. Sopyan, *Int J Photoenergy.,* 2009, Article ID 962783, 8 pages.

[45] R. Sasikala, V. Sudarsan, C. Sudakar, R. Naik, T. Sakuntala and S. R. Bharadwaj, *Int. J. Hydrogen Energy.*, 2008, 33, 4966.

[46] Q. Li, B. Guo, J. Yu, J. Ran, B. Zhang, H. Yan and J. R. Gong, *J. Am. Chem. Soc*., 2011, doi.org/10.1021/ja2025454.

[47] X. Li, J. Yu, J. Low, Y. Fang, J. Xiaoc and X. Chen, *J. Mater. Chem. A.,* 2014, 10.1039/c4ta04461d.

[48] J. A. Navio, G. colon, M. I. Litter and G. N. Bianco, *J. Mol. Catal. A: Chem.,* 1996, 106, 267.

[49] R. R. Lieten, Epitaxial growth of nitrides on germanium, VUB University Press, 2009.

[50] K. U. Minchitha and R. G. Balakrishna, *Mater. Chem. Phys.,* 2012, 136, 720.

Figure captions:

- **Figure 1:** Experimental set up to measure the H_2 evolution.
- **Figure 2:** X-ray diffraction pattern of $FeTiO_2$ nanoparticles.
- **Figure 3:** FE-SEM image of the synthesized $FeTiO_2$ nanoparticles.

- **Figure 4**. HRTEM images of the prepared $FeTiO_2$ nanostructures a & b) facets of Ti and Fe c) dislocation and inset SAED pattern d) Fe induced titania, inset histogram of particle size distribution e) Fe_2O_3 adsorbed titania f) over lie of nanoparticles.
- **Figure 5:** Energy-dispersive X-ray spectra of $FeTiO_2$. (Inset: Atomic and elemental percentage of the dopant in titanium dioxide).
- **Figure 6:** XPS spectrum of Fe doped TiO_2 photocatalyst a) $FeTiO_2$ spectrum b) Ti 2p core level c) O 1S core level d) Fe 2p core level.
- **Figure 7:** UV-visible absorption spectra for (a) Commercial TiO_2 (b) $FeTiO_2$. Inset indicates the effect of dopant concentration on absorption threshold.
- **Figure 8:** Reflectance spectra of $FeTiO_2$ photocatalyst.
- **Figure 9**: Photoluminescence spectra of (a) CM-TiO_2, (b) $FeTiO_2$, (c) $FeTiO_2$ and sacrificial agent.
- **Figure 10:** H_2 evolution from 0.15 % $FeTiO_2$ (a) pH=6 (b) pH=8 (c) pH=10.
- **Scheme 1:** Schematic representation of electronic band structure of the synthesized photocatalyst.

Table 1. Surface area, crystallite size and cell volume of photocatalysts.

Element	Crystallite size	Cell volume	Surface area
TiO_2	30 nm	137.1 $Å^3$	24.67 m^2/g
$FeTiO_2$	59 nm	138.0 $Å^3$	48.85 m^2/g

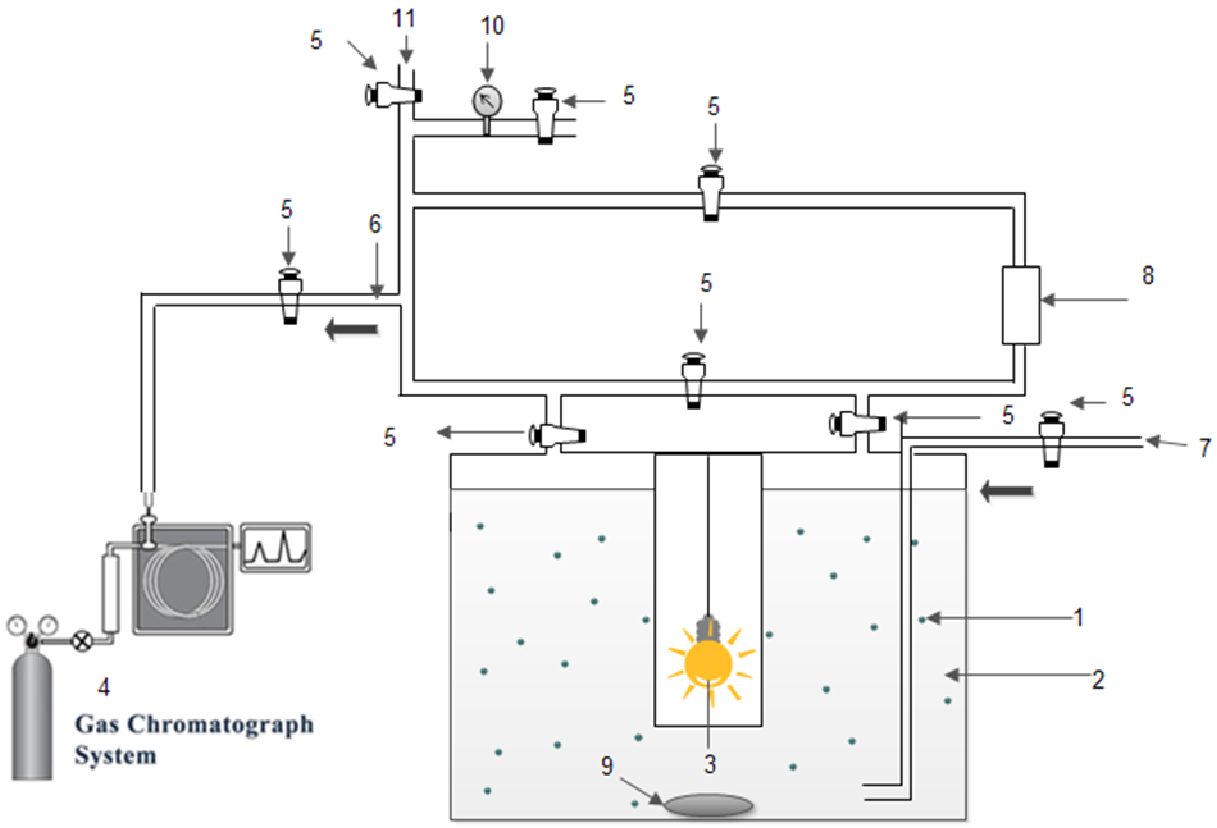

Figure 1. Experimental set up to measure the H_2 evolution

1. Powder Particles
2. Solution
3. Light Source
4. Gas Chromatograph System
5. Stopcock
6. Outlet Valve
7. Inlet Valve
8. Circulation pump
9. Magnetic Stirrer
10. Pressure Gauge Pump

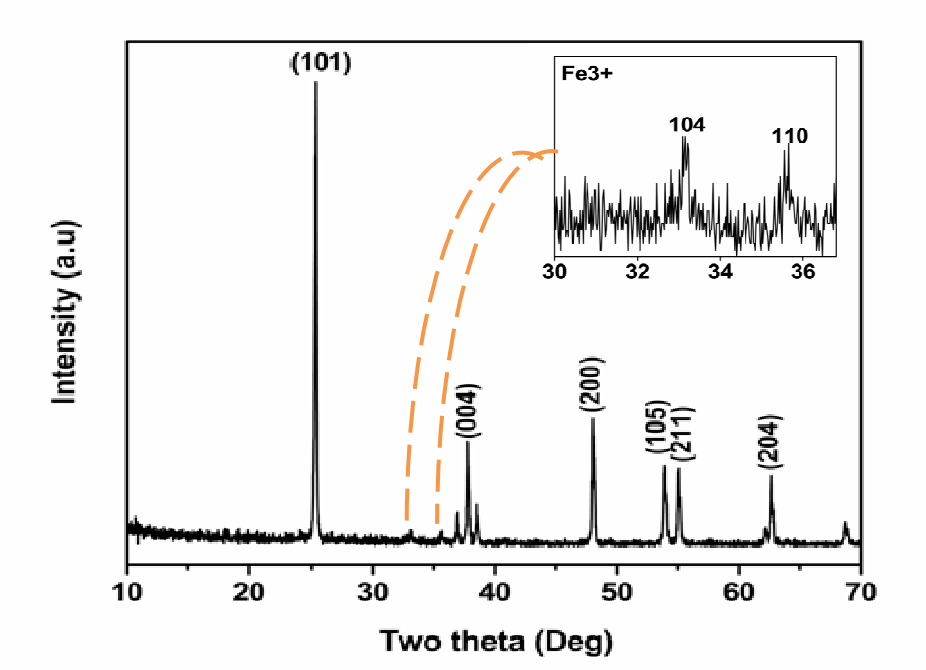

Figure 2. X-ray diffraction pattern of $FeTiO_2$ nanoparticles.

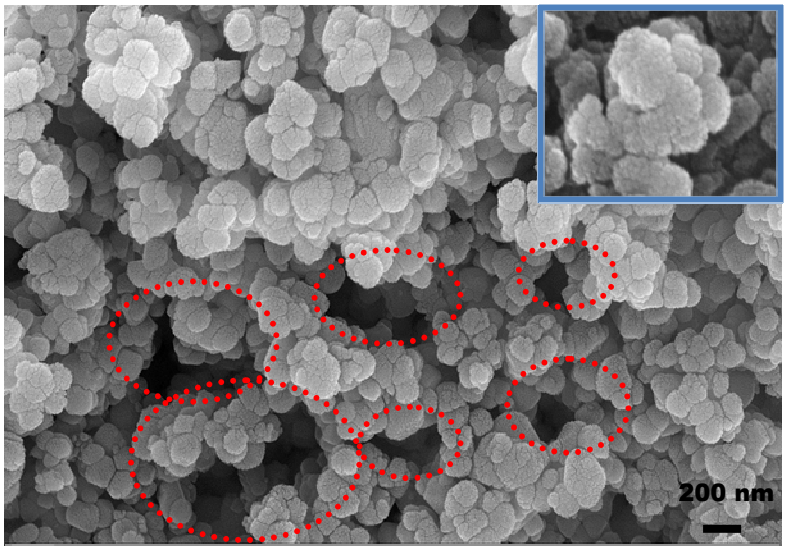

Figure 3: FE-SEM image of the synthesized $FeTiO_2$ nanoparticles.

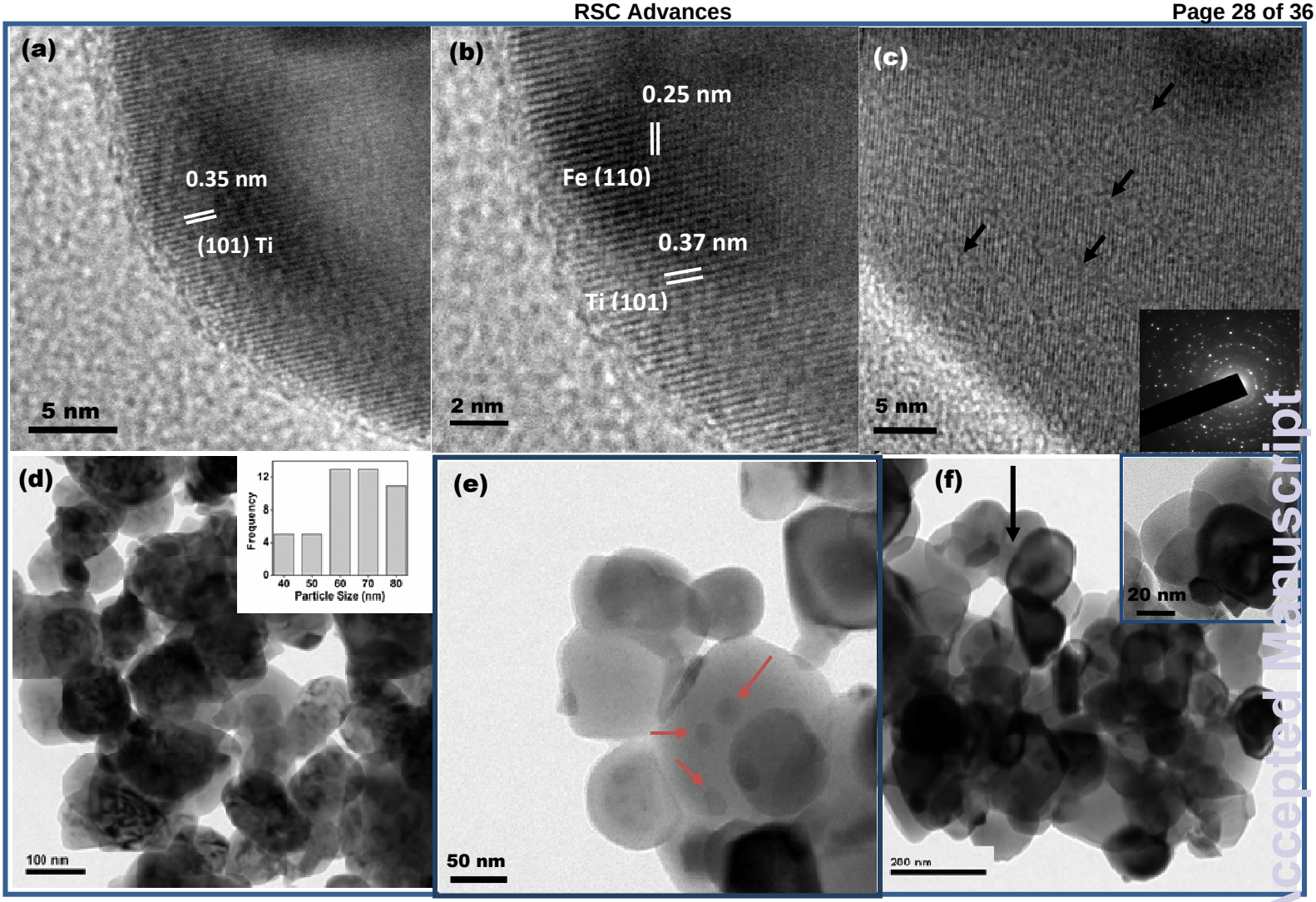

Figure 4. HRTEM images of the prepared $FeTiO_2$ nanostructures a & b) facets of Ti and Fe c) dislocation and inset SAED pattern d) Fe induced titania, inset histogram of particle size distribution e) Fe_2O_3 adsorbed titania f) over lie of nanoparticles.

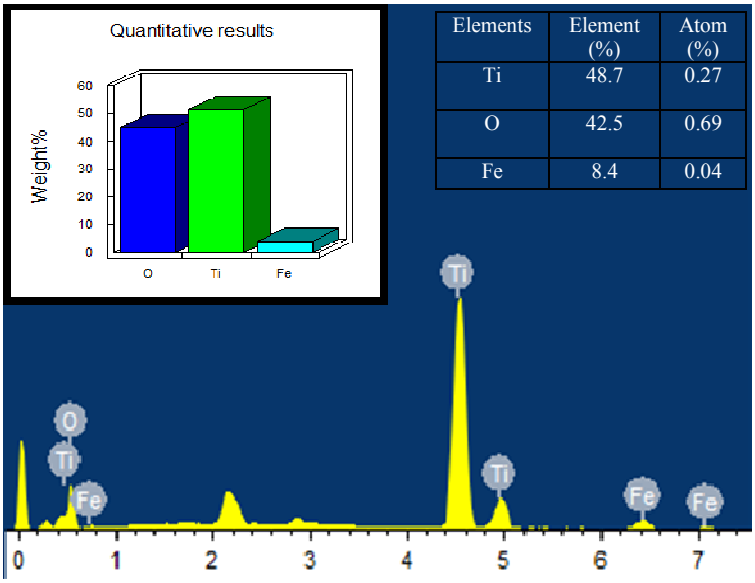

Figure 5. Energy-dispersive X-ray spectra of $FeTiO_2$. (Inset: Atomic and elemental percentage of the dopant in titanium dioxide)

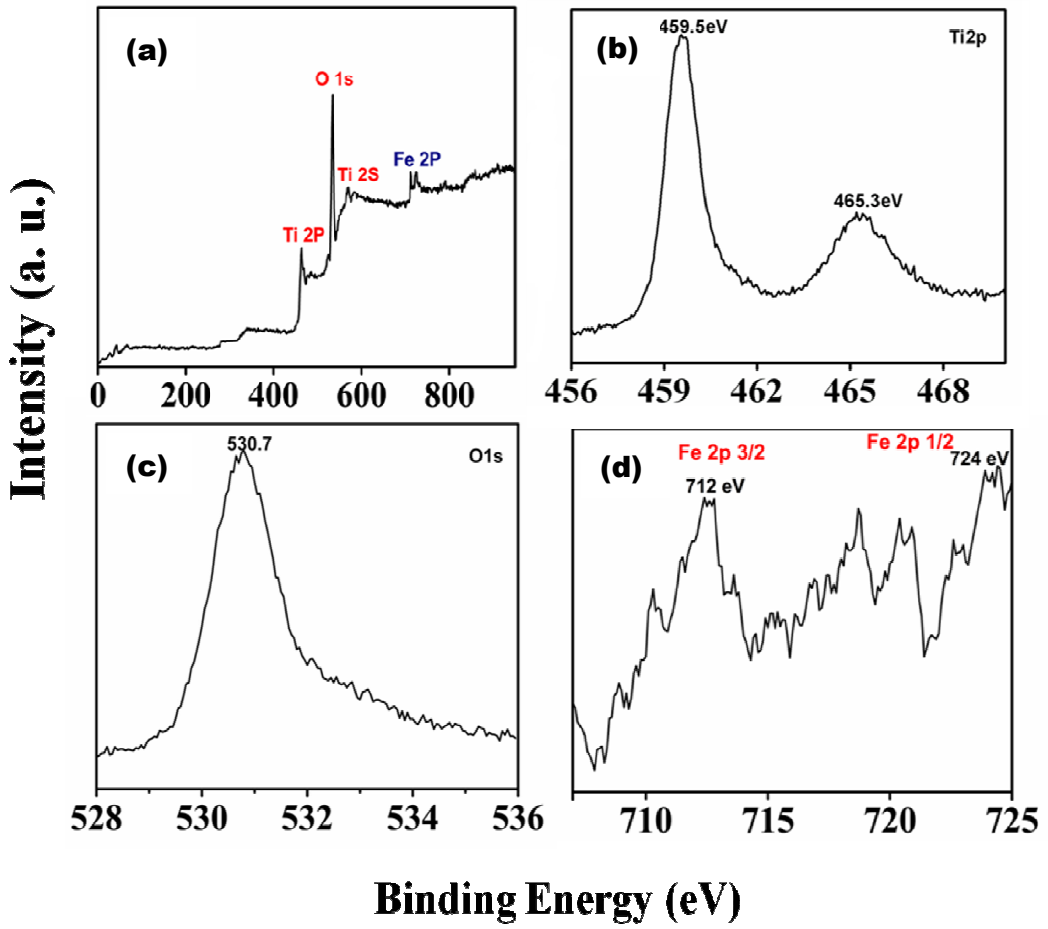

Figure 6. XPS spectrum of Fe doped TiO_2 photocatalyst a) $FeTiO_2$ spectrum b) Ti 2p core level c) O 1S core level d) Fe 2p core level

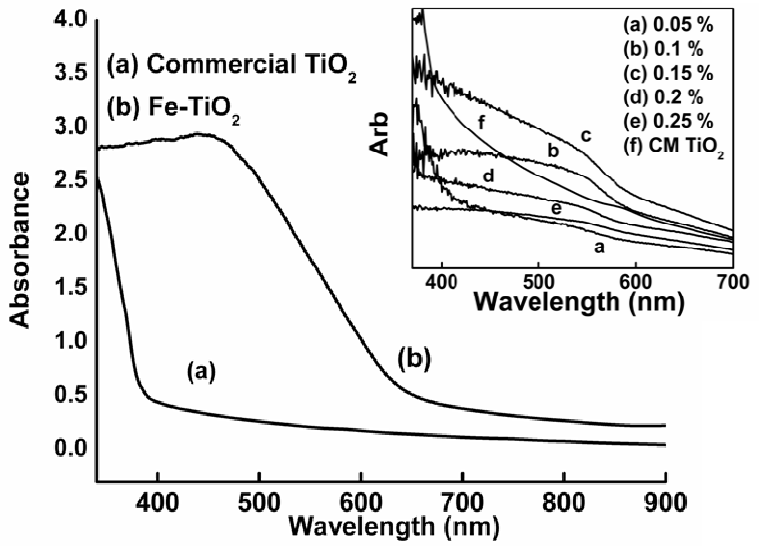

Figure 7. UV-visible absorption spectra for (a) Commercial TiO_2 (b) $FeTiO_2$. Inset indicates the effect of dopant concentration on absorption threshold

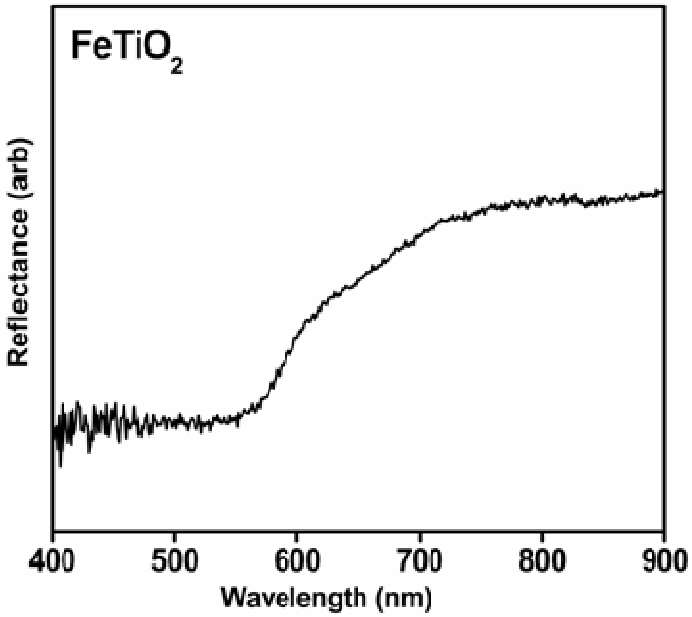

Figure 8. Reflectance spectra of $FeTiO_2$ photocatalyst.

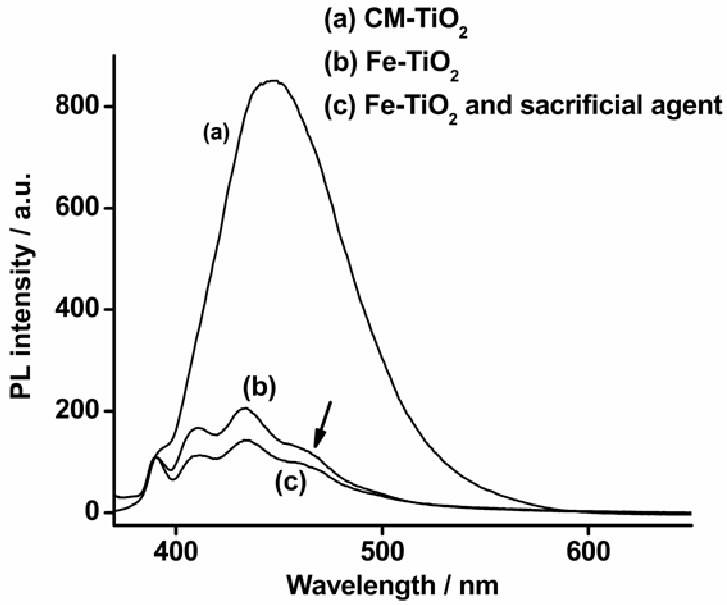

Figure 9. Photoluminescence spectra of (a) CM-TiO_2, (b) $FeTiO_2$, (c) $FeTiO_2$ and sacrificial agent

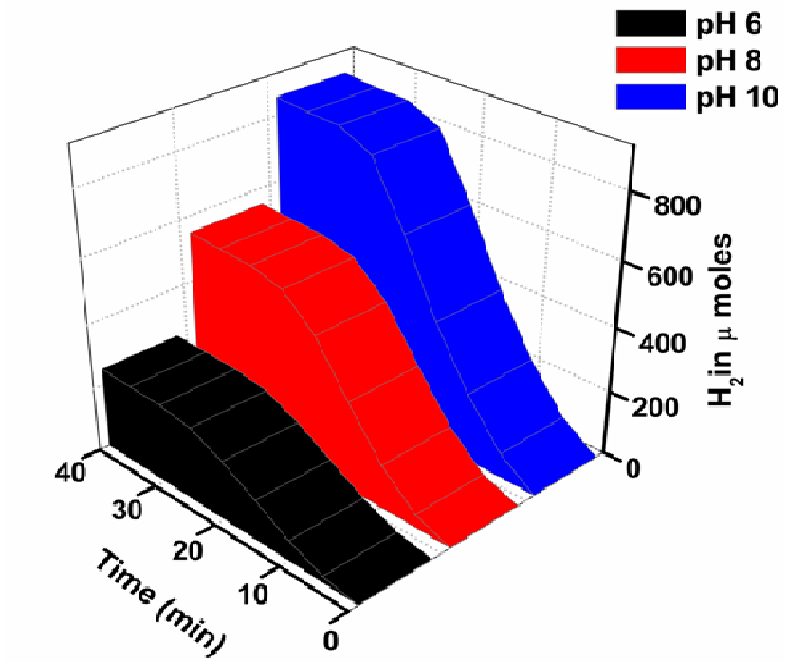

Figure 10. H_2 evolution from 0.15 % $FeTiO_2$ (a) pH=6 (b) pH=8 (c) pH=10

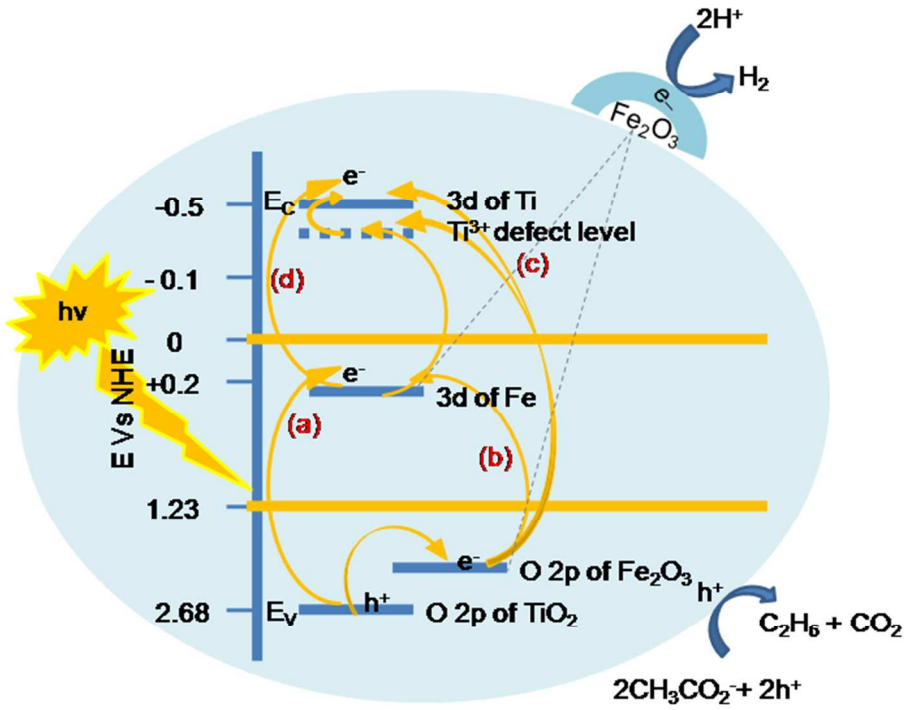

Scheme 1. Schematic representation of electronic band structure of the synthesize photocatalyst.

Graphical Abstract:

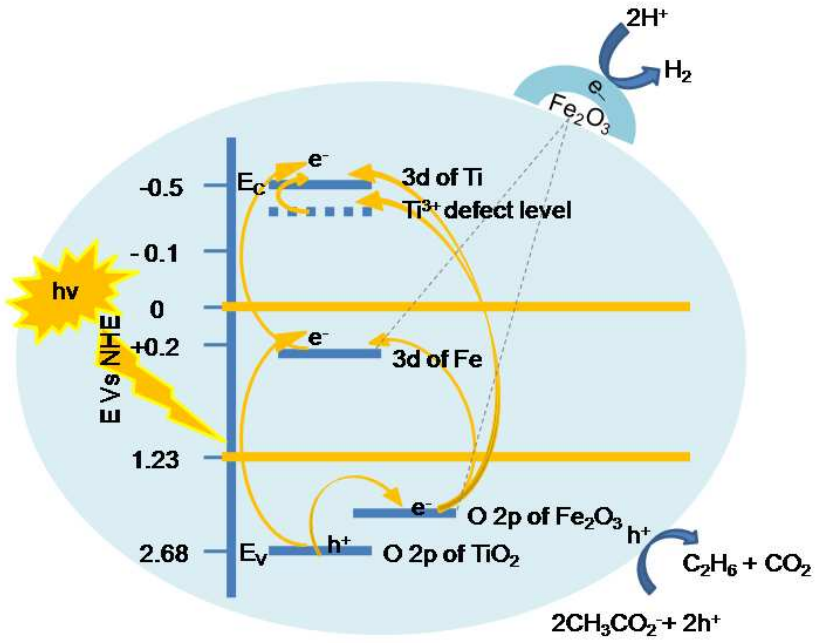

Titania as doped and coupled semiconductor with Fe and Fe_2O_3 respectively, allows favorable alignment of band edges for remarkable hydrogen evolution.